PROCEEDINGS OF SCIENCE

Exploring the Impact of Variabilities in Relativistic Jets dynamics

Zakaria Meliani,[a] **Félix Tornatore,**[a] **Gaëtan Fichet de Clairfontaine**[b] **and Andreas Zech**[a]

[a] *Laboratoire Univers et Théories, Observatoire de Paris, Université PSL, Université de Paris cité, CNRS, F-92190 Meudon, France*

[b] *Julius-Maximilians-Universität Würzburg, Fakultät für Physik und Astronomie, Emil-Fischer-Str. 31, D-97074 Würzburg, Germany; gaetan.fichet-de-clairfontaine@physik.uni-wuerzburg.de*

E-mail: zakaria.meliani@obspm.Fr

Relativistic jets, fast and collimated outflows that propagate over large distances, are commonly observed in various astrophysical objects, including active galactic nuclei (AGN), microquasars, and pulsars. These jets exhibit variability, which we study through scenarios involving complex periodic and flicker noise. Our goal is to deepen our understanding of the underlying physics of these observed variabilities. To achieve this, we use special relativistic simulations. In particular, we use the AMRVAC code to handle the fluid dynamics and follow the evolution of the electron population. In addition, we analyze and interpret synthetic images from radio to X-ray using the REPTIDE code. Our investigation focuses on the dynamics of variable jets, and our results show for the first time that rapid jet variability can lead to the development of large quasi-steady shocks.

High Energy Phenomena in Relativistic Outflows VIII
23-26 10 2023
Paris, France

PoS(HEPROVIII)039

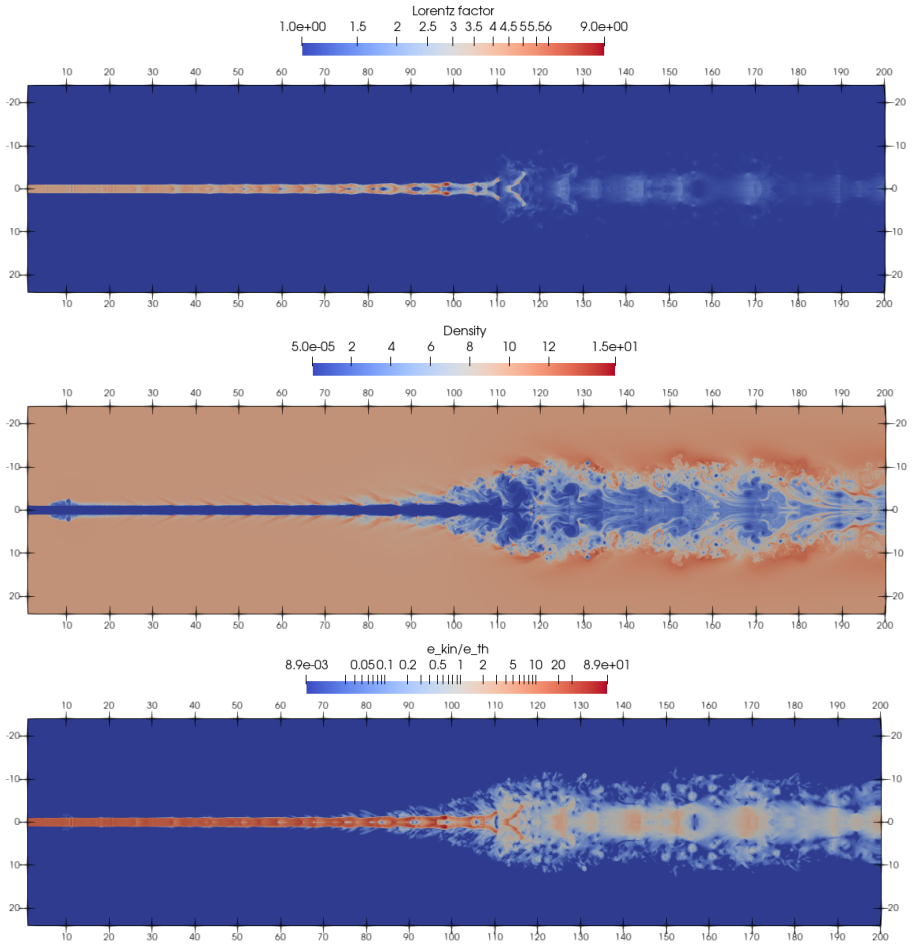

Figure 1: Snapshot of the jet at $t = 600R_{jet}/c$. First: Lorentz factor map. Second: Density map. Third: e_{kin}/e_{th} map.

Several observational surveys of relativistic astrophysical jets have provided compelling evidences of their emission across the entire electromagnetic spectrum, ranging from radio waves to the high-energy Γ-ray band (Boccardi et al. (2017); Zensus (1997)) Moreover, these jets have been found to be associated with cosmic rays (H. E. S. S. Collaboration et al. (2020)). Furthermore, these jets commonly display variability in their emissions across all wavelengths. The timescales of this variability decrease as the observed frequency increases, from the radio (Wehrle et al. (2012)) to the Γ-ray band (Abramowski et al. (2012)). A common approach to fitting the variability observed in the light curves is to employ a flicker noise signal Malzac (2013), which demonstrates a power spectral density inversely proportional to the frequency. This type of signal is frequently observed in natural systems exhibiting stochastic behavior. The investigation of the underlying mechanisms responsible for this variability remains a subject of ongoing debate within the field of astrophysics. The variability observed in relativistic jets can be attributed to a variety of factors, contributing to the intricate nature of these phenomena. Magnetic reconnection processes have been identified as one potential source of variability (Tramacere et al. (2011); Werner et al. (2018)), while instabilities and shear layers within the jet can also lead to fluctuations in the emission (Stawarz & Petrosian

(2008)). Additionally, the precession of the jet itself has been observed and studied (Britzen et al. (2019)). Internal shocks, resulting from variations in plasma velocity or density, have been proposed as another mechanism (Fichet de Clairfontaine et al. (2021)), leading to changes in the emission properties and resulting in flux fluctuations. Furthermore, external factors such as the presence of companion objects or interactions with the interstellar medium can contribute to the observed variability in relativistic jets.

1. Model

We utilize the special relativistic version of the `AMRVAC` code Keppens et al. (2012), which allows us to simulate the evolution of a perfect fluid governed by the conservation equations of mass, momentum, and energy,

$$\partial_t D + \nabla \cdot (D, \mathbf{v}) = 0, \tag{1}$$

$$\partial_t \mathbf{S} + \nabla \cdot (\mathbf{S}\mathbf{v} + p) = 0, \tag{2}$$

$$\partial_t \tau + \nabla \cdot ((\tau + p)\,\mathbf{v}) = 0\,. \tag{3}$$

Here, $D = \Gamma\rho$ represents the density in the laboratory frame, where Γ denotes the Lorentz factor ($\Gamma = \sqrt{1/(1-v^2)}$). The density in the comoving frame is denoted by ρ, while $\mathbf{v}$ represents the three-vector velocity, and p denotes the thermal pressure. The momentum is given by $\mathbf{S} = \Gamma D h \mathbf{v}$, where $h = 1 + e_{th} + p/\rho$ represents the enthalpy with e_{th} being the thermal energy. Additionally, $\tau = \Gamma D h - p - D$ is a function of the total energy. To close the system of equations, we adopt the Synge equation of state (Meliani et al. 2004) and corresponding polytropic index at low temps temperature is $\gamma = 5/3$.

1.1 Injection variability

In order to investigate the scenario of internal shocks, we introduce a time variability in the Lorentz factor at the base of the jet. We initially choose to use a complex periodic variability, which is constructed by summing sinusoidal waves with different amplitudes and frequencies. The complex periodic variability pattern is particularly interesting as it exhibits packets of high-amplitude oscillations that are modulated by a higher-frequency oscillation. This pattern allows for the formation of distinct regions of enhanced activity within the jet. More precisely we chose the complex periodic variability to maintain continuity with the work of (Pjanka & Stone (2018)), which focused on over-dense jet cases. In our study, we specifically investigate under-dense jet scenarios, which are more relevant for relativistic jets. The description we use the Lorentz factor is

$$\Gamma_{\rm jet} = \max\left(\Gamma_{,\rm mean} + \frac{\sum_{i=1}^{N}(\Gamma_i - \Gamma_{,\rm mean})\sin(\omega_i\, t)}{N}, \Gamma_{\rm jet,floor}\right), \tag{4}$$

With Γ_i, the amplitude of the fluctuation, and ω_i, the associated sinusoidal frequency, are chosen uniformly from the ranges $[\Gamma_{\rm min}, \Gamma_{\rm max}]$ and $[\omega_{\rm min}, \omega_{\rm max}]$, respectively. Within the pattern, the number of sinusoidal fluctuations is denoted by N.

We also investigate the model of the Lorentz variability as a flickering variability. We use such variability to mimic the observed multiwavelength light curves, with the aim of reproducing them.

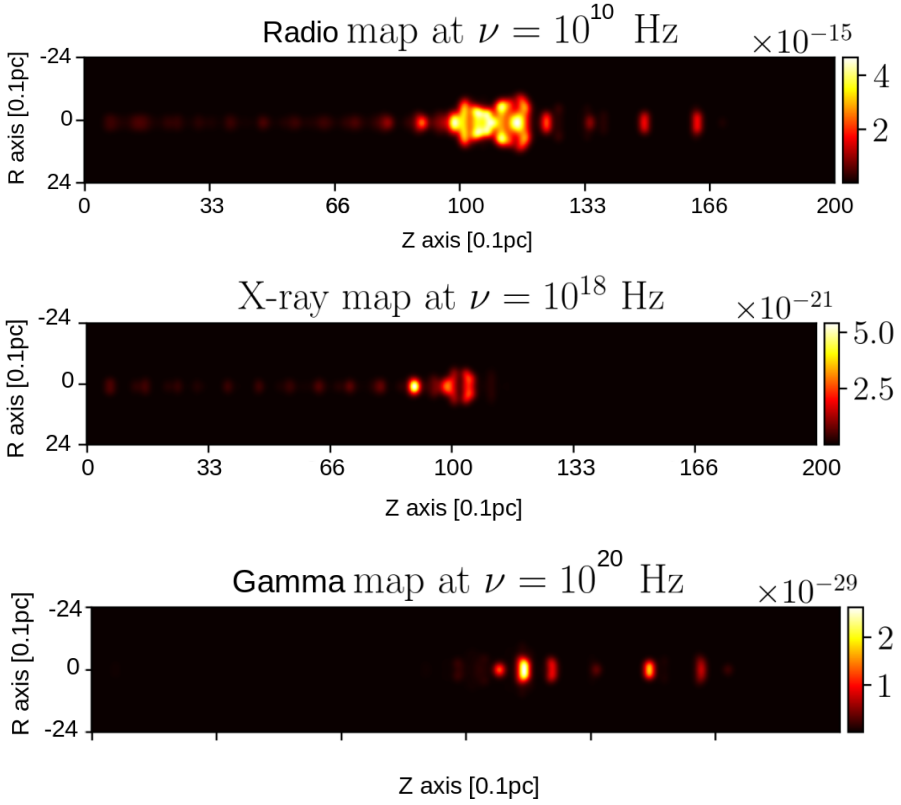

Figure 2: Synthetic image of the jet with complex periodic variability at: (top) $\nu = 10^{10}$ Hz (Radio), (midel) $\nu = 10^{18}$ Hz (X-rays), (down) at $\nu = 10^{20}$ Hz (γ - rays). We use $R_{jet} = 0.1$ pc, $z = 0.00428$, and $\theta = 90°$. The unit of the colorbar is erg.cm^{-2}.s^{-1}.

The method to generate such variability in described in (Malzac 2013; Timmer & Koenig 1995). Specifically, we consider a power density function for the variability frequency ω which range from $[\omega_{\min}, \omega_{\max}]$. As result, the fluctuation in the Lorentz factor is fonction of the time t and has a Fourrier power density spectrum $S(w)\, \alpha\, w^{-1}$.

2. Shock Dynamics in Variable Jets

The simulations reveal that similar dynamics are induced in both cases. The variability leads to the formation of moving shock regions, which are sustained and amplified by the flow and compression waves. At a distance of approximately 150 R_{jet}, high-amplitude shock waves converge, collide, and instigate the formation of a quasi-stationary large shock region (see Figure 1). This region thermalizes and decollimates the jet. Despite the type of variability, the general behavior remains consistent. The primary difference between a variable jet with flickering variability and one with complex periodic variability lies in the zone of moving shock. In the case of complex periodic variability, powerful shocks are equidistant, whereas in the case of flickering variability, they are non-equidistant. Indeed, the distribution of the moving shock regions is no longer periodic but random along the jet, reflecting the random variations of the flickering variability.

3. Synthetic images & comparison with observations

Using the RIPTIDE code, we produce synthetic images of the jet, i.e., maps of the non-thermal emissions as we could observe them from Earth for jets deformed by complex periodic variability and flicker noise variability. The purpose is to observe the non-thermal emissions coming from moving and stationary shocks caused by the variability and compare them qualitatively with observations. To do so, we consider a standard AGN jet radius: $R_{jet} = 0.1$pc and the redshift of the M87 galaxy: $z = 0.00428$. We produce synthetic images for both complex periodic and flickering variabilities considering an observation angle $\theta = 90°$ (we observe the jet perpendicularly) and for several frequencies (figures 2).

The synthetic images of the jet obtained through Riptide exhibit knots of higher flux intensity. On the X-ray and Radio maps (figure 2), we spot knots of high emissions under $Z = 100R_{jet}$, they correspond to the moving shock regions induced by the variability. In these regions, electrons are accelerated by diffusive shock acceleration and cooled down by the synchrotron process, resulting in a higher flux intensity. Around $Z = 100R_{jet}$, we observe a large high emission region, it coincides with the termination shock. As the termination shock is very strong, the emission is more intense in these regions than on the moving knots. The high emission region is smaller on the X-ray map than on the radio map as high energy particles are more efficiently cooled down than low energy ones, thus they radiate in a smaller zone. In the radio map, we observe knots of higher emission even downstream from the termination shock, they coincide with higher Lorentz factor regions that can be observed in this part of the jet. Downstream the termination shock, the jet radius is increased thus the emission zones are larger than upstream from the termination shock.

On the γ - rays map, the emissions are low in the regions associated with moving shock regions or with the termination shock. This is caused by the effect of relativistic beaming. This effect is increased when the speed of the particle increases and as the synthetic images are done with an observation angle of 90°, a part of the photons do not reach the observer.

References

Abramowski, A., Acero, F., Aharonian, F., et al. 2012, , 746, 151

Boccardi, B., Krichbaum, T. P., Ros, E., & Zensus, J. A. 2017, , 25, 4

Britzen, S., Fendt, C., Zajaček, M., et al. 2019, Galaxies, 7

Fichet de Clairfontaine, G., Meliani, Z., Zech, A., & Hervet, O. 2021, , 647, A77

H. E. S. S. Collaboration, Abdalla, H., Adam, R., et al. 2020, , 582, 356

Keppens, R., Meliani, Z., van Marle, A. J., et al. 2012, Journal of Computational Physics, 231, 718

Malzac, J. 2013, , 429, L20

Meliani, Z., Sauty, C., Tsinganos, K., & Vlahakis, N. 2004, , 425, 773

Pjanka, P. & Stone, J. M. 2018, , 477, 2376

Stawarz, Ł. & Petrosian, V. 2008, , 681, 1725

Timmer, J. & Koenig, M. 1995, , 300, 707

Tramacere, A., Massaro, E., & Taylor, A. M. 2011, The Astrophysical Journal, 739, 66

Wehrle, A. E., Marscher, A. P., Jorstad, S. G., et al. 2012, The Astrophysical Journal, 758, 72

Werner, G. R., Uzdensky, D. A., Begelman, M. C., Cerutti, B., & Nalewajko, K. 2018, , 473, 4840

Zensus, J. A. 1997, , 35, 607